Journal of Materials Chemistry B

Accepted Manuscript

ROYAL SOCIETY OF CHEMISTRY

www.rsc.org/materialsB

Journal of
Materials Chemistry B

RSCPublishing

ARTICLE

^{13}C NMR aided design of molecularly imprinted adsorbents for selectively preparative separation of Erythromycin†

Cite this: DOI: 10.1039/x0xx00000x

Received 00th January 2012,
Accepted 00th January 2012

DOI: 10.1039/x0xx00000x

www.rsc.org/

Yuxin Zhang,[abc] Xue Qu,*[ac] Jinpeng Yu, Liancai Xu,[d] Zhiqiang Zhang,[d] Hua Hong and Changsheng Liu*[abc]

Molecularly imprinted polymers (MIPs) with high binding performance and good selectivity are of interest not only in the field of analytical chemistry, but also in the bio-pharmaceutical industry because of their potential use as affinity sorbents for selectively preparative separation of drug molecules. The choice of suitable functional monomer for template molecule plays a key role in the performance of MIPs. Erythromycin (ERY; $C_{37}H_{67}NO_{13}$; mol.wt.733.9), produced by bio-fermentation, is a representative macrolide antibiotic with multiple polar groups. In the present study, ^{13}C NMR spectroscopy for the first time was employed to evaluate the interactions between ERY and a set of functional monomers at the atomic level. Based on the ^{13}C chemical shifts changes on ERY molecular structure when binding with different functional monomers, the optimal monomer of methacrylic acid (MAA) was selected and the rational binding sites were predicted. A sequence regarding to the interaction force of these binding sites for MAA was proposed, and Density Functional Theory (DFT) theoretical calculation of Lewis basicity of the O/N atoms located at these sites confirmed its reliability. The molecularly imprinted sorbents (MIAs) for ERY were prepared by suspension polymerization method using MAA as functional monomer and ethylene glycol dimethacrylate (EGDMA) as cross linker. The effects of monomer to template ratio and solvent environment employed during the adsorption on the imprinting efficiency of MIAs were both discussed. The adsorption isotherm of ERY onto MIAs was fitted by Langmuir isotherm model. And specific selectivity towards ERY of these materials was confirmed. The optimized MIAs as column packing materials can separate ERY from its crystal mother liquid with high recovery and good selectivity, exhibiting a promising capability for productively separation of ERY in large scale. To our best knowledge, these results firstly indicated ^{13}C NMR spectroscopy is a simple and effective method for the rational design of MIAs towards complex template molecule. The separation model built in this study represents a novel application of MIPs for future industrial production.

Introduction

Molecularly imprinted polymers (MIPs) have attracted considerable interest from scientists and engineers because of their advantages like specific recognition, high stability and ease of mass preparation.[1-5] MIPs are usually prepared by co-polymerizing suitable functional monomers in the presence of desired template molecule. The monomers and template are pre-organized by several possible interactions, such as hydrogen bonding, hydrophobic interaction, Van der Waals force and electrostatic force which determine the spatial arrangement of monomers around the template. After polymerization, the template is removed to leave a chemically and sterically complementary void in the polymer network, which is able to rebind the template specifically. Therefore, monomers which strongly interact with the template should lead to MIPs with high selectivity and rebinding capacity.[2, 3, 6-8] However, very few experimental studies have been carried on prior to polymerization in the attempt to understand these interactions and further to screen functional monomer for template analytes, especially for those with complex multiple polar groups. It is partly because the well-established spectroscopic methods such as FT-IR and UV-Vis spectroscopy

cannot always provide comprehensive and significant signal changes in the monomer-template pre-organization system.[9-12] Other advanced techniques like QCM (Quartz crystal microbalance) and SPR (Surface plasma resonance), however, require tedious template grafting process before the real measurement.[13-18] Therefore, it is a great challenge to develop a convenient and effective method to accurately sense the interactions existing in the pre-organization system and thereby provide a reliable guidance for the rational design of MIPs towards template molecules with complex structure.

NMR spectroscopy has been applied to understand the intermolecular interactions responsible for the formation of monomer-template pre-organization system at the atomic level, because changes in the chemical shift (Δδ) between the free and bound templates can reflect the influence of the monomer binding has on their atomic magnetic environment.[19-22] However, ^{1}H NMR has poor performance when applied for the analysis of targets with complex chemical structure, for the fact that multiplets generating from the coupling and splitting between adjacent chemically non-equivalent ^{1}H atoms would result in very complicated spectra, which cannot be easily interpreted.[23, 24] In contrast to ^{1}H NMR, ^{13}C NMR spectra show a single peak for each carbon atom on the molecule because of the rare couplings occurring between ^{13}C atoms, and the typical range of ^{13}C chemical shifts is much broader for ^{1}H (by a factor of about 20).[25] These two inherent characters determine a higher resolution can be available in ^{13}C NMR spectra than in ^{1}H NMR. Therefore, ^{13}C NMR may be explored as a convenient and robust method for studying the intermolecular interactions in complicated systems.

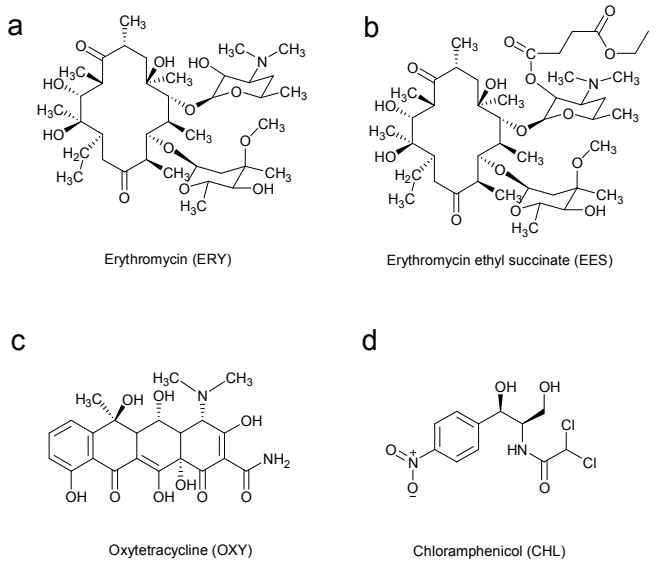

Fig. 1 Chemical structures of (a) Erythromycin (ERY), (b) Erythromycin ethylsuccinate (EES), (c) Oxytetracycline (OXY), (d) Chloramphenicol (CHL)

Erythromycin (ERY; $C_{37}H_{67}NO_{13}$; mol.wt.733.9) is a representative macrolide antibiotics produced by *Saccharopolyspora erythraea* and is widely used to treat gram-positive bacteria and mycoplasma infections. The chemical structure of ERY is a large macrocyclic lactone ring attached with desosamine and cladinose residues (Fig. 1a).[26, 27] Polar groups such as hydroxyl, carbonyl, ester and tertiary amine etc. on ERY molecule are suggestive of potential binding sites involving in the pre-organization events.[9, 10, 28] In bio-pharmaceutical engineering, large-scale industrial separation of ERY has traditionally relied on solvent extraction and subsequent crystallization. It is not clear that these traditional operations are best suited for meeting the emerging demands for higher product purities, energy effective operation, and minimal waste generation.[29, 30] In principle, adsorption offers great potential for separations because adsorbents can be designed with binding sites which confer high selectivities. It is desirable to develop molecularly imprinted adsorbents (MIAs) to offer both high concentrating abilities for effective recovery and sufficient selectivities towards ERY.

In the present study, ^{13}C NMR spectroscopy for the first time was employed to investigate the interactions between ERY and a set of functional monomers at the atomic level. The rational binding sites were proposed and the optimal functional monomer was selected based on the spectroscopic results. The resultant MIAs exhibited good performance to productively separate ERY from its crystal mother liquid, which could be considered promising affinity adsorbents for selectively extracting ERY in industrial-scale.

Experimental

Materials

ERY standard and ERY crystal mother solution were obtained from HEC Pharm Co., Ltd. (Yichang, China). Methacrylic acid (MAA), hydroxyethyl methacrylate (HEMA), acrylamide (AA), methyl methacrylate (MMA), polyvinyl alcohol (PVA) and ethylene glycol dimethacrylate (EGDMA) were purchased from Jingchun Reagent Co., Ltd. (Shanghai, China). All other reagents were of analytical grade and purchased from China Nation Medicines (Shanghai, China).

The "crystal mother solution" is residual liquid from the ERY crystallization process in industrial production, which includes small amounts of ERY and ERY derivatives, some inorganic matters and other unidentified impurities. The solvent is 5%-10% acetone- water mixture.

^{13}C NMR studies

The interactions between different functional monomers and ERY were examined by ^{13}C NMR spectroscopy. ^{13}C NMR spectra of ERY and ERY-functional monomer mixture with the molar ratio of 1:12 in d-$CHCl_3$ were obtained on a NMR spectrometer (AVANCE III 400MHz, Bruker, Germany). The ^{13}C chemical shifts of each carbon atom on ERY and monomer-bound ERY were carefully assigned according to the former report.[31, 32] And Δδ, the values corresponding to the chemical shifts changes of ERY when interacting with functional monomers were calculated.

DFT calculation

Chemical calculations were performed using density functional theory methods of hybrid B3LYP functional with Becke exchange and Lee-Yang-Parr Correlation provided by the Gaussian 03.[33, 34] As a general protocol, geometry optimizations were performed at B3LYP/6-31G(d) theoretical level. Net atomic charges on the O/N atoms, q, of the ERY molecule have been computed from a NBO population analysis on the isolated ERY. The local softness, s^-, relative to the basic character of those O/N atoms, has been computed according to the equation (1).[35]

$$s^- = f^- S = \frac{q^N - q^{N-1}}{IE - EA} \quad (1)$$

where f^- is the Fukui function, S is the global chemical softness, IE is the first ionization energy, EA is the electron affinity energy, q^N is the charge of the O/N atom in the neutral molecule, and q^{N-1} is the charge on the O/N atom in the +1 charged molecule.

Synthesis of the MIAs

The MIAs, specific for ERY were prepared by suspension polymerization using MAA as the functional monomer, EGDMA as the cross-linking monomer and AIBN as the radical initiator. $CHCl_3$ and H_2O were used as the continuous phase and disperse phase, respectively. The synthetic procedure is described as below:

1.0 g of polyvinyl alcohol (PVA) was dissolved in water, then poured into a 1000 mL tree-neck flask in a water bath at 60 °C and was stirred at 400 rpm. (I)

1 mmol of template molecule was first dissolved in chloroform following the addition of a certain amount of MAA, 25 mmol of EGDMA and 120 mg of AIBN. The mixture was then degassed under vacuum for 5 min and purged with nitrogen gas for 10 min. (II)

The solution (II) was added by dropwise into the flask (I) while stirring, and N2 was passed over the flask simultaneously until the end of the reaction. After 24 h polymerization, the adsorbents were sieved into a 50-80 μm fraction and were washed with hot water to remove the PVA from the surface of the materials. Thereafter, the template molecule was extracted from the adsorbents by sequential washing with 1:9 (v/v) acetic acid and methanol mixture followed by washing with methanol until no residue of ERY was found in the rinses. Finally, the purified adsorbents were dried under vacuum for further use. The non-imprinted adsorbents (NIAs) were prepared following the same procedure except the addition of ERY.

Characterization of MIAs

The morphology of the prepared adsorbents was examined by scanning electron microscopy (S-4800, Hitachi, Japan). Specific surface area of adsorbents was detected by surface area and porosimetry analyzer (ASAP2010N, Micromeritics, USA).

Binding experiments

30 mg of MIAs and NIAs were mixed with ERY standard solution for 12 h at 25 °C with continuous shaking. The resultant mixture was then centrifuged at 500 rpm for 2 min. The concentration of the free ERY in the supernatant was measured by sulphuric acid chromogenic method.[36] The amount of ERY bound to the adsorbents was determined by subtracting the amount of free ERY from the amount of ERY initially added. The imprinting factor (IF) was calculated according to the following equation:

$$IF = \frac{B_{MIAs}}{B_{NIAs}} \quad (2)$$

where B (mg·g^{-1}) is the binding capacity.

The selectivity of MIAs was investigated using Chloromycetin (CHL), Oxytetracycline (OXY) and Erythromycin ethylsuccinate (EES) as the structurally related substrates.

To evaluate the adsorption property of the materials in acetonitrile, 30 mg of adsorbents were mixed with ERY standard solution with different concentrations under continuous shaking. The final supernatant was detected to calculate the amount of ERY bound. And Langmuir isotherm analysis was used to estimate the binding characteristics of the materials.

Dynamic adsorption experiment

A given amount (2.0 g) of MIAs was packed into a chromatographic column (5.0 cm × Ø 1.0 cm). The ERY solution of 1.0 mg·mL^{-1} in CH_3CN was allowed to gradually flow through the column at a rate of 1.53 BV·h^{-1}. The effluents were collected with 20 min interval, and the ERY concentrations in the effluents were analysed by sulphuric acid chromogenic method. The dynamic binding curve was plotted, and the leaking adsorption amount and saturated adsorption amount of ERY were calculated with the data of the concentration and bed number of the effluents, respectively. The dynamic binding experiment on NIAs packed column was carried out following the same procedure.

Selectively preparative separation of ERY

In this study, the separation of ERY from its crystal mother solution was carried on MIAs chromatographic column which is the same as mentioned above. In the loading step, the crystal mother solution of appropriate volume was allowed to pass through the column, followed by washing with pure water to delete any aqueous impurity. Then the column was washed with a certain volume of CH_3CN. Column bound ERY was finally eluted using 5 BV of ethanol-ammonia water (9:1, v/v). The flow rate was set at 1.53 BV·h^{-1} during the whole procedure.

The ERY purity in the samples before and after column treatment was determined by HPLC-UV method (2795, Waters, USA). Briefly, a certain amount of loading solution (crystal mother solution) or the eluents were first dried under vacuum. The obtained powder products were dissolved with a concentration of 1.0 mg·mL^{-1}. The samples were then subject to HPLC analysis using C18 column and quantified at 210 nm. The ERY recovery was determined by the comparison of eluted ERY amount to the initially loaded amount.

Furthermore, the purity of the recovered sample was detected by differential-pulse voltammetry (DPV) using the classical three-electrode system on CHI 660D electrochemical workstation (Chenhua, China). The test samples were prepared by dissolving powder products in the electrolyte (0.1M KCl, 10% ethanol) with a final concentration of 1.0 mg·mL^{-1}. The DPV scans of the ERY standard sample with different concentrations were constructed to make a linear calibration curve.

Results and discussion

For non-covalent molecular imprinting, the complementary intermolecular interactions between template and functional monomer are critical factors for precise molecular recognition. NMR experiments can provide detailed information about these interactions. For example, the extent of the observed chemical shifts changes between the free and monomer bound templates is in general proportional to the strength of the interactions.[22] And the location of the atomic nuclei most affected by the monomers may give qualitative information about the binding sites.[37] In this study, interactions between ERY and functional monomers were studied by ^{13}C NMR analysis in the d-$CHCl_3$ solvent environment aiming to find out a suitable monomer for ERY imprinting and to fundamentally understand the

interaction mechanism. The molar ratio of the template to the monomer in NMR solution was fixed at 1:12. Table S1 shows

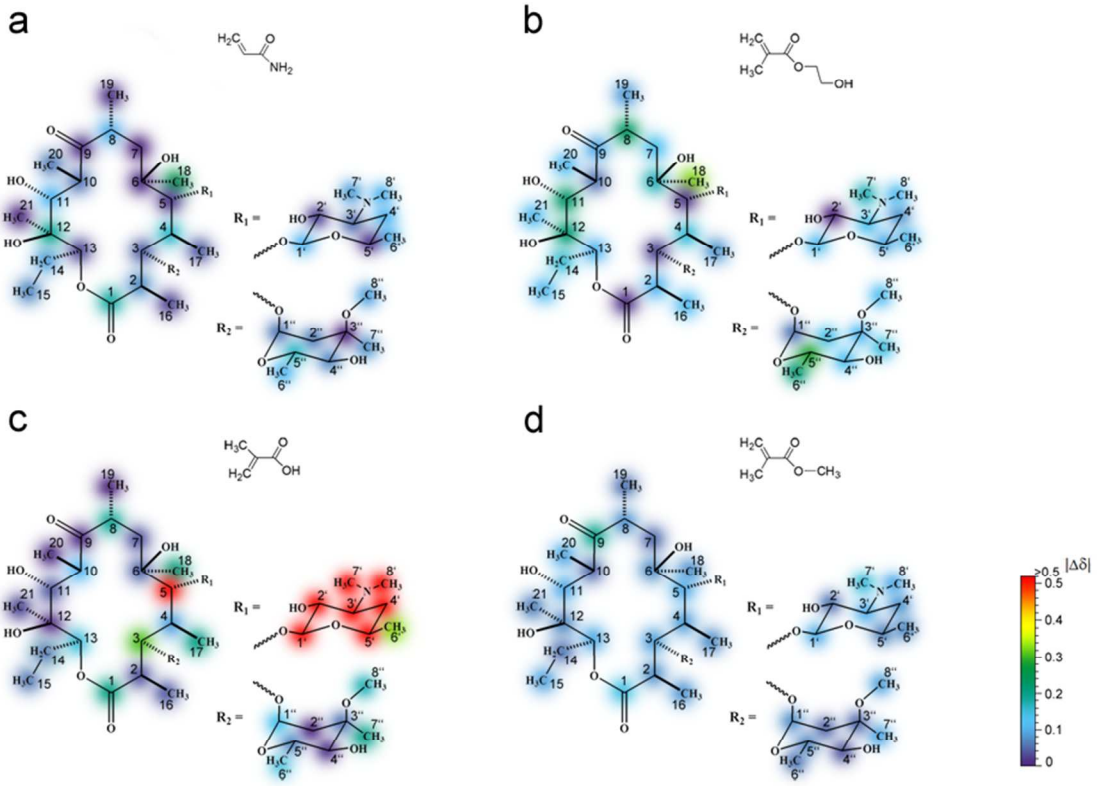

Fig. 2 The absolute value of chemical shift change (|Δδ|) of each C atom on ERY molecular structure: (a) in AA binding system; (b) in HEMA binding system; (c) in MAA binding system; (d) in MMA binding system.

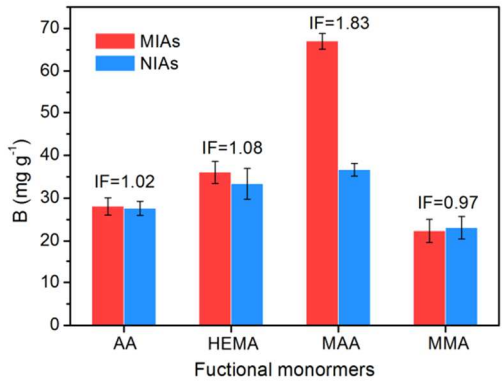

Fig. 3 The imprinting efficiency of MIAs and NIAs synthesized with different functional monomers. ERY to functional monomer mole ratio is 1:12; n = 3.

the concrete values of ^{13}C chemical shifts change Δδ on ERY when interacting with functional monomers. Colourful spots corresponding to the absolute value of Δδ (|Δδ|) on each carbon atom are pictured on the ERY structure formula in Fig. 2, with the purpose to depict the alteration of ERY magnetic environment. It can be seen that the changes of the carbon chemical shifts on ERY in ERY-MAA system are the most significant as a whole, while the addition of AA, MMA and HEMA monomers to the ERY solution did not induce profound changes. This is suggestive of the strongest interactions occurring between ERY and MAA with the typical functional group of –COOH. Being a system in equilibrium, the stronger interactions between the template and the functional monomer determine a more stable template-monomer preorganization system, which results in an increase in the number of specific binding sites created during the polymerization. We conducted synthetic experiments to further testify the performance of the four functional monomers for ERY imprinting. A series of imprinted and non-imprinted polymers were synthesized using AA, MMA, HEMA and MAA as the functional monomers respectively and EGDMA as the cross linker. The imprinting efficiency of the resulted materials for ERY was investigated (Fig. 3). It was revealed that imprinted polymers formed with the functional monomer of MAA presented not only the highest binding amount but also the highest imprinting efficiency towards ERY with respect to control polymer. In contrast, imprinted materials made from AA, MMA, HEMA all showed lower efficiency and binding capacity. The imprinting factors (*IF*), calculated by taking the ratio of equilibrium binding capacity of MIPs to that of NIPs, for AA, HEMA, MAA and MMA are 1.02, 1.08, 1.83 and 0.97, respectively. These results are in good agreement with the conclusion we draw from ^{13}C NMR results that MAA is indeed the optimal candidate for ERY imprinting.

Furthermore, we predicted the possible MAA binding sites on ERY molecule. As mentioned before, the presence of multiple polar groups such as hydroxyl, carbonyl, ester, ether and tertiary amine on ERY have potential for participating the intermolecular binding process. The changes of carbons chemical shifts near these groups can provide reliable information to understand the binding events. In Table S1, one can see a range of -1.49~2.00 ppm shifts of a number of

resonances arising from carbon atoms (C_3', C_4', C_7', and C_8' etc.) in the vicinity of the basic tertiary nitrogen (–$\overset{/}{N}$–). The relatively large shift of these atoms indicated that protonation of the tertiary amine (–$\overset{/}{N}H^+$–) and subsequent interaction, presumably by ion pairing with the COO^- anion, resulting in a significant change in the magnetic environment of adjacent carbon atoms. Other dramatic change in chemical shift about 1.14 ppm was observed at C_5, which maybe also resulted from the influence of protonation of the tertiary amine. A downfield shift about 0.31 ppm for C_3 was observed demonstrated a possible H-bond formed between the O atom (C_3–O–C_1") and the H atom on –COOH of MAA. Two O atoms on the ester group (C_1(O)O–C_{13}) are also considered to engage H-bond with MAA, since the changes of chemical shifts corresponding to the adjacent C_1 and C_{13} atoms were both observed, 0.21 ppm for C_1 and 0.15 ppm for C_{13}. As for C_{11}, C_{12}, C_6 and C_4" all attached with –OH group, the corresponding chemical shifts almost have no change, probably meaning a very weak intermolecular force between –OH and MAA. However, in some case –OH group is believed to not only accept but also give a H-bond to –COOH group in Sanglar's research.[38]

As a whole these results confirm that multiple binding sites involve in the ERY-MAA preorganization system. Electrostatic and H-bonding interactions appear to be major effects contributing to the stability of this structure. Since the largest chemical shift change corresponds to the strongest interaction, the Δδ values near these binding sites suggest a possible sequence regarding to their interaction force with –COOH of MAA molecule, as follows: –$\overset{/}{N}$– > C_3–O–C_1" > C_1(O)O–C_{13} > C_1(O)O–C_{13} > –OH ≈ O=C_9.

Table 1 The local Softness s^- of O/N atoms on ERY.

	s^- (e·mol·J^{-1})	|Δδ| of adjacent C		
–$\overset{/}{N}$–	-2.95×10^{-6}	1.01 (C_3')	1.16 (C_7')	1.11 (C_8')
C_3–O–C_1"	-1.72×10^{-6}		0.31 (C_3)	0.14 (C_1")
C_1(O)O–C_{13}	-1.68×10^{-6}			0.21 (C_1)
C_1(O)O–C_{13}	-1.45×10^{-6}		0.21 (C_1)	0.15 (C_{13})
C_9=O	-2.00×10^{-6}			0.01 (C_9)
C_{11}–OH	-2.11×10^{-6}			0.04 (C_{11})

From the viewpoint of Lewis acid-base theory, the binding process in the ERY-MAA system can be regarded as the donation and acception of an electron pair between O/N on ERY and active H on MAA. Therefore, in order to assess the reliability of this sequence, the local softness, s^-, relative to the basic character of those O/N atoms, has been computed using DFT calculations.[39, 40] This approach is used to gauge the Lewis basicity of atoms in molecules as it has already been successfully used in numerous previous studies.[41, 42] In Table 1, the tertiary N atom (–$\overset{/}{N}$–) was revealed to have the strongest Lewis basicity, with the s^- of -2.95×10^{-6} e·mol·J^{-1}. When looking at the O atoms located at C_3–O–C_1" and C_1(O)O–C_{13}, the s^- values were estimated at -1.72×10^{-6}, -1.68×10^{-6}, and -1.45×10^{-6} e·mol·J^{-1}, respectively. The more basicity of O/N atoms, the stronger it may interact with the active H on MAA molecule. The values of s^- given in Table 1 reproduce the trend relative to the interaction force predicted from ^{13}C NMR shifts. However, strong basic properties were also found on O atoms, for example located at C_9 (O=C_9) and C_{11} (HO–C_{11}), with the s^- values of -2.00×10^{-6} and -2.11×10^{-6} e·mol·J^{-1}, respectively. This is not in accordance with the results of ^{13}C NMR shifts changes |Δδ| for the corresponding C atoms, where almost no changes were observed. This is probably because these polar groups form stable intramolecular H-bonds. They could not participate in the H-bond formation with active H coming from guest MAA molecule.[43]

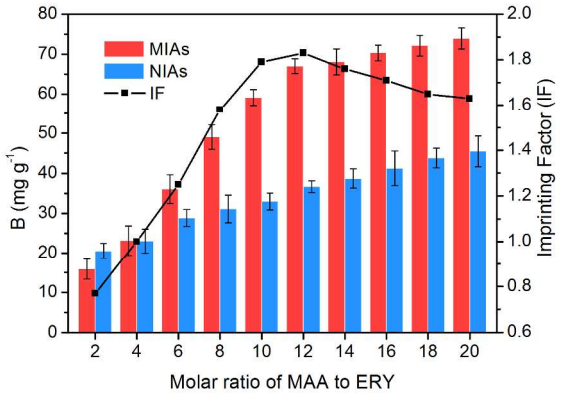

Fig. 4 Binding capacity and imprinting factors of MIAs and NIAs with different molar ratios of MAA to ERY.

The molar relationship between the functional monomer and the template is also a critical factor for precise molecular recognition in non-covalent molecular imprinting.[28] In order to further optimize the polymer's formulation, we synthesized a series of MIAs and the corresponding NIAs with varying molar ratios of MAA to ERY. The imprinting performance of the resultant MIAs and NIAs is presented in Fig. 4. As we can see, the binding capacity of MIAs for ERY increased obviously with the increase of the molar ratio of MAA to ERY up to 12, and then reached to a plateau. The IF also increased gradually and the maximum value of 1.83 appeared at the ratio of 12:1, and a decrease was observed when over-dosage of MAA existing in the polymer matrix. These results support the prevalent opinion that high molar ratios of monomer to template raise the percentage of non-specific binding, while low ratios produce insufficient binding sites, both of which will lower the memory ability of the MIAs.[44] The greatest imprinting effect of MIAs can be generated only with the optimal proportion of template to monomer. In this study, the optimized molar ratio of MAA to ERY was confirmed as 12:1. The corresponding imprinted polymers and non-imprinted polymers were chosen for the following experiments.

Meanwhile, the structures of MIAs and NIAs were studied by SEM. As shown in Fig. 5a, b, d and e, MIAs and NIAs prepared by suspension polymerization both exhibited spherical morphology, homogeneously distributed and well proportional. The diameter of these beads was estimated at around 70 μm. The amplified pictures of MIAs (Fig. 5c) and NIAs (Fig. 5f) revealed nanoporous surfaces, which may be ascribed to the porogenation of $CHCl_3$ solvent used in the polymerization. The BET analysis listed in Table 2 indicated a pore size of 5.89 nm for MIAs, and 7.45 nm for NIAs. MIAs exhibited slightly lower porosity than NIAs. The total pore volume of MIAs was determined at 0.51 cm^3·g^{-1}, while it was 0.72 cm^3·g^{-1} for NIAs. Similarly, surface area of MIAs also seemed smaller than that of NIAs, with values of 336 m^2·g^{-1} and 380 m^2·g^{-1}, respectively. These results prove that the specific adsorption behavior of

MIAs for template molecule has no relationship to their individual pore structure.

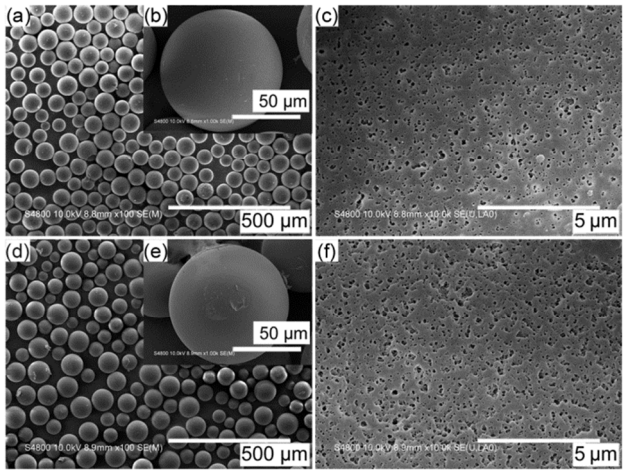

Fig. 5 Scanning electron microscopy (SEM) images of MIAs and NIAs prepared by suspension polymerization with a diameter of *ca.*70 μm and nanoporous surface: (a, b, c) MIAs and (d, e, f) NIAs.

Table 2 Pore structure analysis of MIAs and NIAs by Brunauer-Emmet-Teller (BET) method.

Adsorbents	Surface area ($m^2 \cdot g^{-1}$)	Total pore volume ($cm^3 \cdot g^{-1}$)	Pore size (nm)
MIAs	336.09	0.51	5.89
NIAs	379.15	0.72	7.45

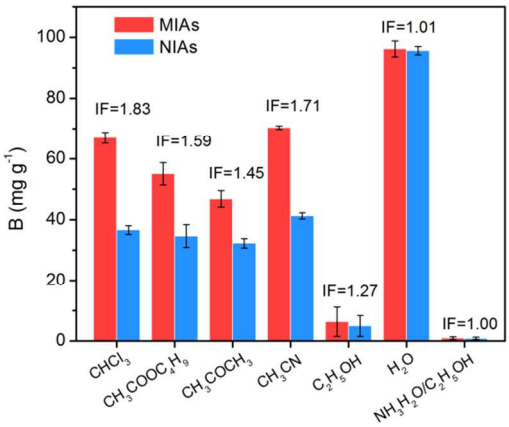

Fig. 6 Binding capacity and imprinting factors of MIAs and NIAs working in different solvents.

The nature of solvent used for the binding experiment also influences the expression of MIAs imprinting effect. In this work, binding performance including binding capacity and IF values of these materials was evaluated in $CHCl_3$, CH_3CN, $CH_3COOC_4H_9$, CH_3COCH_3, C_2H_5OH and H_2O respectively. The results are shown in Fig. 6. As expected, an obvious imprinting effect with IF value of 1.83 was demonstrated in $CHCl_3$. Being the porogen for ERY MIAs synthesis, $CHCl_3$ facilitates the high complementation between ERY and imprinted cavities formed in the MIAs. CH_3CN, as a polar aprotic solvent, is also inert to the interactions by H-bonding and ion paring occurring in the matrix, which would result in a similar adsorption amount and imprinting feature compared to $CHCl_3$. In the case of CH_3COCH_3 and $CH_3COOC_4H_9$, however, the specific affinities of MIAs for ERY were both weakened. It is attributed to their proton accepting capability that interrupts the H-bond formation between ERY and MIAs partly, thereby weakening the memory ability of MIAs and their adsorption capacity. In C_2H_5OH solvent, the adsorption amount of ERY both on MIAs and NIAs significantly decreased. Ethanol has strong H-donoring capability,[20] by which the formation of H-bond between ERY and the adsorbents would be weakened or even completely blocked. Therefore the access of ERY to the binding sites was greatly suppressed. Ionic interaction, although not being disturbed by C_2H_5OH, cannot trigger the specific binding event due to its nondirectional feature.[45] This may be served as an interpretation for the observed poor IF value of 1.27 for MIAs working in C_2H_5OH solution. The addition of $NH_3 \cdot H_2O$ into C_2H_5OH further lowered the adsorption capacity of these materials down to zero. Indeed, since NH_3 has strong basic property, it may compete with tertiary nitrogen (–N–) on ERY to bind the $–COO^-$ on MAA molecule, thereby disrupting the ERY-MAA interaction by ion paring. However, when H_2O was used as the single solvent, both MIAs and NIAs presented high binding capacity for ERY. The occurrence of nonspecific hydrophobic interaction between ERY and adsorbents is responsible for this phenomenon probably.[46]

The adsorption isotherm studies are of fundamental importance in clarifying the nature of adsorption behavior. In this study, the adsorption isotherms of MIAs and NIAs for ERY were evaluated in CH_3CN solvent respectively with the initial ERY concentration ranging from 0.2 to 1.6 $mg \cdot mL^{-1}$. As shown in Fig. 7, MIAs adsorbed much more ERY than NIAs at each concentration. The adsorption capacity increased with the increase of ERY amount in the initial solution. A saturated state was reached to for both adsorbents when the ERY concentration was over 1.2 $mg \cdot mL^{-1}$. The Langmuir isotherm model was used to interpret the adsorption behavior of these materials. The Langmuir isotherm is based on an assumption of monolayer adsorption onto a surface containing a finite number of adsorption sites and uniform energies of adsorption with no transmigration of adsorbate in the plane of the surface.[47] The Langmuir isotherm is governed by the following equation:

$$\frac{1}{Q_e} = \frac{1}{Q_m} + \frac{1}{Q_m k} \cdot \frac{1}{C_e} \quad (3)$$

Where Q_e and C_e are the equilibrium concentration of ERY on adsorbent and in solution respectively. Q_m and k are Langmuir constants related to the maximum adsorption capacity and dissociation equilibrium constant respectively.

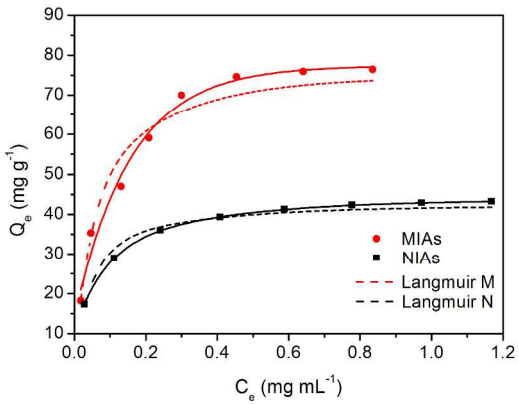

Fig. 7 Adsorption isotherms of MIAs and NIAs for ERY. Temperature: 25°C; solvent: CH_3CN.

The dash line shown in Fig. 7 indicated that the Langmuir equation fitted well for ERY adsorption over the entire range of concentrations. The values of the isotherm constants calculated from the slope and intercept of the plots using regression analysis are shown in Table 3. The predicted Q_m and k of MIAs exhibited the superiority over NIAs as ERY adsorbents. The high correlation coefficient (R^2) further confirmed the validity of the Langmuir isotherm model.

Table 3 Langmuir isotherm constants of MIAs and NIAs.

Adsorbents	Q_m (mg·g^{-1})	k (mL·mg^{-1})	R^2
MIAs	79.11	15.80	0.9908
NIAs	43.33	23.41	0.9882

It has been reported that the effect of isotherm shape can predict if an adsorbent is "favorable" or "unfavorable".[47] The essential features of the Langmuir isotherm can be expressed in terms of a dimensionless constant separation factor or equilibrium parameter, E_L, which is defined by:

$$E_L = \frac{1}{1 + kC_0} \quad (4)$$

where C_0 is the initial ERY concentration (mg·mL^{-1}). The parameter E_L>1, E_L=1, 0<E_L<1, E_L=0 indicates the isotherm shape as unfavorable, linear, favorable and irreversible, respectively. The E_L values given in Table 4, shows that both the MIAs and NIAs is favorable adsorbents for ERY.

Table 4 E_L values based on the Langmuir equation.

Initial concentration (mg·mL^{-1})	E_L	
	MIAs	NIAs
0.2	0.240	0.176
0.4	0.137	0.096
0.6	0.095	0.066
0.8	0.073	0.051
1.0	0.060	0.041
1.2	0.050	0.034
1.4	0.043	0.030
1.6	0.038	0.026

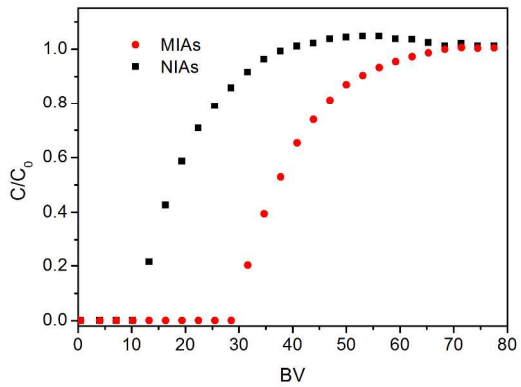

Fig. 8 Dynamic adsorption curves of MIAs and NIAs for ERY. Initial concentration: 1.0 mg·mL^{-1}; flow rate: 1.53 BV·h^{-1}.

In order to further investigate the adsorption properties of MIAs and NIAs, the adsorption experiment was also performed in the column model. Fig. 8 displays the dynamic adsorption curves of MIAs and NIAs for ERY solution of 1.0 mg·mL^{-1} in CH_3CN respectively. As the ERY solution flowing throughout the column, the breakthrough curve of ERY in MIAs packed column was observed to be clearly different from that for NIAs column. The leaking volume for MIAs was estimated to be 28 BV, whereas 10 BV for NIAs, having a difference of 18 BV. By calculation, the leaking and saturated adsorption amounts of MIAs column are 54.95 mg·g^{-1} and 76.66 mg·g^{-1}, respectively, whereas for NIAs column are 19.63 mg·g^{-1} and 38.36 mg·g^{-1}, respectively. These results once again display that the MIAs have a higher adsorption capacity for ERY compared to NIAs. Dynamic binding model was proved to be a powerful method for clarifying the difference between MIAs and NIAs control because of the increased plate numbers.

Table 5 Q_e and K_d of substrates on MIAs and NIAs under equilibrium binding conditions.

Adsorbates	Q_e (mg·g^{-1})		K_d (mL·g^{-1})	
	MIAs	NIAs	MIAs	NIAs
ERY	76.46	43.16	324.81	75.93
EES	48.61	42.36	94.59	73.49
CHL	1.05	1.08	1.10	1.10
OXY	25.91	23.23	35.00	30.30

The selectivity tests of MIAs were carried out under equilibrium binding conditions by using ERY, EES, CHL and OXY as contrasting adsorbates. Their chemical structures are listed in Fig. 1. The equilibrium adsorption capacity (Q_e) and the distribution coefficient (K_d) of the selected adsorbates between solution and MIAs are listed in Table 5. K_d is defined as:

$$K_d = \frac{Q_e}{C_e} \quad (5)$$

Where Q_e (mg·g^{-1}) and C_e (mg·mL^{-1}) are the equilibrium concentration of ERY on adsorbent and in solution respectively.

Results showed that the adsorbed amount of ERY onto MIAs was much higher than that of contrasting regents, with the value of 76.46 mg·g^{-1}. The corresponding values of K_d gave the same tendency, the maximum K_d of 324.81 mL·g^{-1} was observed for ERY adsorption. MIAs exhibited better recognition capability for ERY templates compared to all other adsorbates, even for the EES molecule with close similarity to the template in the way of functional groups arrangement and molecular size. On the other hand, NIAs showed low Q_e and K_d for all the regents. These results indicate that the imprinting process created microcavities with good memory for template molecule in the present study. Contrastive regents did not have complementary shape or chemical structure with these cavities and multiple interaction strength could not be produced within the cavities, thereby reducing the binding capability towards these molecules.

The separation of ERY from its crystal mother liquid at preparative scale was performed in the large chromatographic column made with a MIAs bed. For the effective separation of ERY from industrial products, solvents employed for the loading, washing and elution steps respectively should be determined carefully. In this study, pristine ERY crystal mother liquid (aqueous solution) was used as the loading solvent, in which all the ERY molecules were ensured to be bound into the column quantitatively (100% adsorption), mainly driven by hydrophobic interactions. A following washing step to wash off the nonspecifically adsorbed components and improve purity

level. It is because CH_3CN was confirmed to supply an insert environment for ERY specific adsorption according the results

Table 6 ERY recovery from the crystal mother solution on MIAs packed column[a].

Sample	$[ERY]_{in}$ (mg·mL^{-1})	P_{in}[b] (%)	Volume loaded (mL)	Washing solvent (BV)	Elution solvent (BV)	P_{out}[c] (%)	Recovery[d] (%)	
crystal mother solution	3.06	39.25	100	20	5	48.91	41.64	MIAs
						40.22	9.72	NIAs
	1.97	39.25	100	20	5	61.23	64.48	MIAs
						53.82	13.59	NIAs
	1.33	39.25	100	20	5	73.34	91.98	MIAs
						59.22	14.81	NIAs
	1.33	39.25	50	20	5	79.26	97.49	MIAs*
						63.47	29.29	NIAs
	1.33	39.25	50	15	5	77.53	97.6	MIAs
						62.93	37.87	NIAs
Standard ERY	1.00	97.60	100	20	5	97.62	98.48	MIAs
						97.22	27.4	NIAs

[a] column size 5.0 cm × Ø1.0 cm; flow rate 1.53 BV·h^{-1}.
[b] the purity of initial ERY, means the percentage of total ERY in the dried product of crystal mother solution.
[c] the purity of recovered ERY, means the percentage of total ERY in the dried product of eluent.
[d] Recovery: (amount of desorbed ERY)/(amount of loaded ERY).

in Fig. 6. A mixed solvent of $C_2H_5OH/NH_3·H_2O$ (9:1, v/v) was employed as the elution solvent to desorb bound ERY from the column, since in this solvent the adsorption of MIAs towards ERY was completely blocked as shown in Fig. 6. Samples flowing throughout the column were monitored by UV-Vis spectrophotometric method. The ERY purity (ERY weight percent in dried sample) before and after the column treatment ($[P]_{in}$ and $[P]_{out}$) and ERY recovery were evaluated and shown in Table 6.

Apparently the separation performance of the column for ERY was found to be governed by the initially loaded sample amount. The ERY recovery was enhanced along with the decrease of the loaded mother liquid. When the column was spiked with ERY mother liquid at 3.06, 1.97 and 1.33 mg·mL^{-1} with the same volume of 100 mL, the MIAs chromatographic column gave recoveries of 41.64, 64.48 and 91.98%, respectively. Meanwhile, the corresponding ERY purities in dried samples were all raised greatly after chromatographic fractionation. With the same parameters, however, the NIAs column gave poor recovery for ERY, indicating the weak retention capacity for ERY in contrast to MIAs. We further lowered the ERY loading quantities down to 50 mL with 1.33 mg·mL^{-1} concentration, the recover and purity of ERY after MIAs column treatment increased up to 97.49% and 79.26%, respectively. The volume of CH_3CN used in the washing step also influences the separation efficiency towards ERY, because a compromise exists between the interference removal and target molecules bleeding. The recovery of ERY washed by 15 BV was estimated at 97.60%, slightly higher than that of 97.49 % for 20 BV CH_3CN, however, insufficient washing in the former treatment resulted in a lower ERY purity of 77.53%, compared to 79.26% for the later condition, which means the volume of washing solvent should be adjusted carefully to meet the specific separation requirement.

The differential-pulse voltammetry (DPV) method offers great scope for the determination of electroactive substances with biological significance.[48, 49] In our study, the ERY purity of the column treated sample in test group MIAs* (Table 6) was further detected by DPV method. As shown in Fig. 9a, the ERY standard samples, within the locatable ambit of concentration, have significant oxidation peaks at around 0.88 V. And the peak current was observed to be proportional to the concentration of ERY standard. A linear calibration curve was obtained for ERY in ranges of 0.4~1.0 mg·mL^{-1}, the insert as shown in Fig. 9b. The MIAs column treated sample exhibited a typical ERY peak, which represented an ERY concentration of 0.8 mg·mL^{-1} determined from the calibration curve. The purity of ERY in the test sample was estimated at 80% (wt.%), showing a high agreement with the result determined by chromatographic method (79.26%). What posed a sharp contrast was that no obvious ERY peak appeared in the sample prepared directly from crystallization mother solution, which is attributed to the presence of too much interference in the crude sample. It disturbed the precise detection by DPV. The eluent obtained from test group MIAs* (Table 6) was also detected by HPLC method directly. The result showed that the recovered ERY achieved a high purity (Fig. S1).

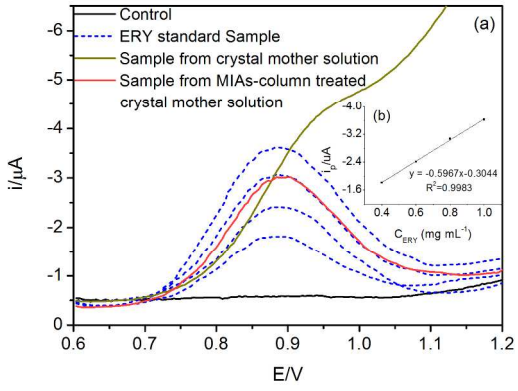

Fig. 9 (a) Differential pulse voltammograms of different ERY samples. (b) The calibration plot oxidation peak current vs. concentrations of ERY.

As a whole, these results indicate that the MIAs chromatographic column contrasting with NIAs column has superior concentration capability and good selectivity for ERY molecule in very complicated systems, which presents attractive application prospects for the quantitatively productive separation of ERY from its fermentation intermediates.

Conclusions

In contrast to optimization by trial and error, ^{13}C NMR analysis was used for the first time to characterize intermolecular interactions in the monomer-template pre-organization stage with the purpose to screen functional monomer for ERY imprinting. MAA was considered as the best monomer because the attached –COOH group can arise the strongest ^{13}C chemical shifts changes on ERY molecule structure, when compared to other monomer candidates. Synthetic experiments also confirmed that MIAs formed with the component of MAA is superior to all other polymers in adsorption capacity and selectivity. Additionally, the NMR data demonstrated that multiple binding sites involve in the ERY-MAA pre-organization formation. Electrostatic and hydrogen bonding interactions contribute to the stability of this system. A sequence regarding to the interaction force of the predicted binding sites for MAA was proposed, which showed a similar tendency with that determined by DFT theoretically calculation. These results indicate that ^{13}C NMR study is a convenient and effective method for understanding the intermolecular interactions especially for some structurally complicated system, and could be applied widely for the development and optimization of imprinting techniques.

Using MAA as functional monomer and EGDMA as cross linker in $CHCl_3$, the ERY MIAs were prepared by suspension polymerization method. The MIAs with 1:12 optimum ratio of ERY to MAA showed the highest adsorption capacity and the best imprinting efficiency for ERY. The solvent effect on the imprinting performance of MIAs was discussed, and CH_3CN and $C_2H_5OH/NH_3{\cdot}H_2O$ were selected as the washing and elution solvents respectively for chromatography separation of ERY. The adsorption isotherm studies of MIAs in CH_3CN indicated a Langmuir isotherm model. The MIAs working in CH_3CN environment presented good discrimination of ERY from other antibiotics. The MIAs were used as chromatographic column packing materials for selective and productive separation of ERY from its crystal mother liquid and showed high enrichment capability and good selectivity for ERY molecules under the optimal conditions.

Acknowledgements

We acknowledge the financial support from Shanghai Natural Science Foundation (11ZR1409100), the National Natural Science Foundation of China (5110304, U1024209), the National Basic Research Program of China (973 Program, 2012CB933600), Innovation Program of Shanghai Municipal Education Commission (14ZZ060), the Fundamental Research Funds for the Central Universities (WD1214056) and Outstanding Youth Fund of East China University of Science and Technology (YD0157109).

Notes and references

[a] The State Key Laboratory of Bioreactor Engineering, East China University of Science and Technology, Shanghai 200237, PR China.

[b] Key Laboratory for Ultrafine Materials of Ministry of Education, East China University of Science and Technology, Shanghai 200237, PR China.

[c] Engineering Research Centre for Biomedical Materials of Ministry of Education, East China University of Science and Technology, Shanghai 200237, PR China.

[d] Department of Material and Chemical Engineering, Zhengzhou University of Light Industry, Zhengzhou 450002, Henan, PR China.

† Electronic Supplementary Information (ESI) available: ^{13}C NMR data. See DOI: 10.1039/b000000x/

1. C. Wang, M. Howell, P. Raulji, Y. Davis and S. Mohapatra, *Advanced functional materials*, 2011, **21**, 4423-4429.
2. Y. Ma, Y. Zhang, M. Zhao, X. Guo and H. Zhang, *Chemical communications*, 2012, **48**, 6217-6219.
3. Y. Zhuang, H. Luo, D. Duan, L. Chen and X. Xu, *Analytical and bioanalytical chemistry*, 2007, **389**, 1177-1183.
4. T. Zhu, D. Xu, Y. Wu, J. Li, M. Zhou, T. Tian, Y. Jiang, F. Li and G. Li, *Journal of Materials Chemistry B*, 2013.
5. C. J. White, M. K. McBride, K. M. Pate, A. Tieppo and M. E. Byrne, *Biomaterials*, 2011, **32**, 5698-5705.
6. H. Zeng, Y. Wang, C. Nie, J. Kong and X. Liu, *The Analyst*, 2012, **137**, 2503-2512.
7. C. He, Y. Long, J. Pan, K. Li and F. Liu, *Journal of Materials Chemistry*, 2008, **18**, 2849-2854.
8. S. Xu, H. Lu, X. Zheng and L. Chen, *Journal of Materials Chemistry C*, 2013, **1**, 4406-4422.
9. S. Song, A. Wu, X. Shi, R. Li, Z. Lin and D. Zhang, *Analytical and bioanalytical chemistry*, 2008, **390**, 2141-2150.
10. Z. Zhang, X. Yang, H. Zhang, M. Zhang, L. Luo, Y. Hu and S. Yao, *Journal of chromatography. B, Analytical technologies in the biomedical and life sciences*, 2011, **879**, 1617-1624.
11. A. Gomez-Caballero, A. Guerreiro, K. Karim, S. Piletsky, M. A. Goicolea and R. J. Barrio, *Biosensors & bioelectronics*, 2011, **28**, 25-32.
12. S. Li, Y. Ge, A. Tiwari, S. Wang, A. P. F. Turner and S. A. Piletsky, *Journal of Catalysis*, 2011, **278**, 173-180.
13. X. Kan, Q. Zhao, Z. Zhang, Z. Wang and J. J. Zhu, *Talanta*, 2008, **75**, 22-26.
14. M. Lotierzo, O. Y. Henry, S. Piletsky, I. Tothill, D. Cullen, M. Kania, B. Hock and A. P. Turner, *Biosensors & bioelectronics*, 2004, **20**, 145-152.
15. M. Bompart, Y. De Wilde and K. Haupt, *Advanced materials*, 2010, **22**, 2343-2348.
16. J. Matsui, M. Takayose, K. Akamatsu, H. Nawafune, K. Tamaki and N. Sugimoto, *The Analyst*, 2009, **134**, 80-86.
17. J. Alenus, A. Ethirajan, F. Horemans, A. Weustenraed, P. Csipai, J. Gruber, M. Peeters, T. J. Cleij and P. Wagner, *Analytical and bioanalytical chemistry*, 2013, **405**, 6479-6487.
18. K. Reimhult, K. Yoshimatsu, K. Risveden, S. Chen, L. Ye and A. Krozer, *Biosensors & bioelectronics*, 2008, **23**, 1908-1914.
19. S. Wu, L. Tan, G. Wang, G. Peng, C. Kang and Y. Tang, *Journal of chromatography. A*, 2013, **1285**, 124-131.
20. N. W. Turner, E. V. Piletska, K. Karim, M. Whitcombe, M. Malecha, N. Magan, C. Baggiani and S. A. Piletsky, *Biosensors & bioelectronics*, 2004, **20**, 1060-1067.
21. E. V. Piletska, M. Romero-Guerra, I. Chianella, K. Karim, A. P. F. Turner and S. A. Piletsky, *Analytica Chimica Acta*, 2005, **542**, 111-117.
22. Z. Xu, L. Liu and Q. Deng, *Journal of pharmaceutical and biomedical analysis*, 2006, **41**, 701-706.
23. J. Courtois, G. Fischer, S. Schauff, K. Albert and K. Irgum, *Analytical chemistry*, 2006, **78**, 580-584.
24. J. O'Mahony, A. Molinelli, K. Nolan, M. R. Smyth and B. Mizaikoff, *Biosensors & bioelectronics*, 2005, **20**, 1884-1893.
25. S. A. Richards and J. C. Hollerton, *Essential practical NMR for organic chemistry*, Wiley. com, 2010.
26. M. Pendela, S. Beni, E. Haghedooren, L. Van den Bossche, B. Noszal, A. Van Schepdael, J. Hoogmartens and E. Adams, *Analytical and bioanalytical chemistry*, 2012, **402**, 781-790.
27. J. Kreusch and R. Bextermoller, *Current medical research and opinion*, 2000, **16**, 1-7.
28. L. Geng, X. Kou, J. Lei, H. Su, G. Ma and Z. Su, *Journal of Chemical Technology & Biotechnology*, 2012, **87**, 635-642.
29. G. J. Lye and D. C. Stuckey, *Chemical Engineering Science*, 2001, **56**, 97-108.
30. Q. Le, L. Shong and Y. Shi, *Separation and Purification Technology*, 2001, **24**, 85-91.
31. J. C. Martins, R. Willem, F. A. Mercier, M. Gielen and M. Biesemans, *Journal of the American Chemical Society*, 1999, **121**, 3284-3291.
32. M. Pendela, S. Béni, E. Haghedooren, L. Van den Bossche, B. Noszál, A. Van Schepdael, J. Hoogmartens and E. Adams, *Analytical and bioanalytical chemistry*, 2012, **402**, 781-790.

33. A. D. Becke, *The Journal of Chemical Physics*, 1993, **98**, 5648.
34. C. Lee, W. Yang and R. G. Parr, *Physical Review B*, 1988, **37**, 785.
35. D. Qi, L. Zhang, L. Wan, Y. Zhang, Y. Bian and J. Jiang, *Physical Chemistry Chemical Physics*, 2011, **13**, 13277-13286.
36. Y. Sun, J. Zhu, K. Chen, S. Zhu and J. Xu, *Front. Chem. Eng. China*, 2008, **2**, 353-360.
37. J. W. Steed and J. L. Atwood, *Supramolecular chemistry*, John Wiley & Sons, 2009.
38. C. Sanglar, T. Jansen, M. C. Silaghi, J. Mernier, P. Mignon and H. Chermette, *Analytical chemistry*, 2012, **84**, 4481-4488.
39. K. Fukui, *Science*, 1982, **218**, 747-754.
40. R. G. Parr and W. Yang, *Density-functional theory of atoms and molecules*, Oxford university press, 1989.
41. H. Chermette, *Journal of computational chemistry*, 1999, **20**, 129-154.
42. P. Geerlings, F. De Proft and W. Langenaeker, *Chemical reviews*, 2003, **103**, 1793-1873.
43. A. Hassanzadeh, J. Barber, G. A. Morris and P. A. Gorry, *The journal of physical chemistry. A*, 2007, **111**, 10098-10104.
44. D. A. Spivak, *Advanced drug delivery reviews*, 2005, **57**, 1779-1794.
45. W. Wan, M. Biyikal, R. Wagner, B. Sellergren and K. Rurack, *Angewandte Chemie International Edition*, 2013.
46. R. L. Malcolm and P. MacCarthy, *Environment International*, 1992, **18**, 597-607.
47. D. Çimen, E. Akbulut, G. Demirel and T. Caykara, *Reactive and Functional Polymers*, 2009, **69**, 655-659.
48. V. Beni, M. Ghita and D. W. Arrigan, *Biosensors & bioelectronics*, 2005, **20**, 2097-2103.
49. P. Manivel, M. Dhakshnamoorthy, A. Balamurugan, N. Ponpandian, D. Mangalaraj and C. Viswanathan, *RSC Advances*, 2013, **3**, 14428-14437.

Based on the ^{13}C chemical shifts changes, the optimal monomer of MAA was selected and the rational binding sites were predicted. The resultant materials show good selectivity for Erythromycin.